ACCOUNTS of chemical research

Article

pubs.acs.org/accounts

Chirality in Thiolate-Protected Gold Clusters

Stefan Knoppe*,† and Thomas Bürgi*

Département de Chimie Physique, Université de Genève, 30 Quai Ernest-Ansermet, 1211 Genève 4, Switzerland

CONSPECTUS: Over recent years, research on thiolate-protected gold clusters $Au_m(SR)_n$ has gained significant interest. Milestones were the successful determination of a series of crystal structures ($Au_{102}(SR)_{44}$, $Au_{25}(SR)_{18}$, $Au_{38}(SR)_{24}$, $Au_{36}(SR)_{24}$, and $Au_{28}(SR)_{20}$). For $Au_{102}(SR)_{44}$, $Au_{38}(SR)_{24}$, and $Au_{28}(SR)_{20}$, intrinsic chirality was found. Strong Cotton effects (circular dichroism, CD) of gold clusters protected by chiral ligands have been reported a long time ago, indicating the transfer of chiral information from the ligand into the cluster core.

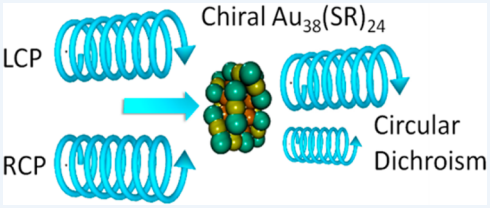

Our lab has done extensive studies on chiral thiolate-protected gold clusters, including those protected with chiral ligands. We demonstrated that vibrational circular dichroism can serve as a useful tool for the determination of conformation of the ligand on the surface of the cluster.

The first reports on crystal structures of $Au_{102}(SR)_{44}$ and $Au_{38}(SR)_{24}$ revealed the intrinsic chirality of these clusters. Their chirality mainly arises from the arrangement of the ligands on the surface of the cluster cores. As achiral ligands are used to stabilize the clusters, racemic mixtures are obtained. However, the separation of the enantiomers by HPLC was demonstrated which enabled the measurement of their CD spectra. Thermally induced inversion allows determination of the activation parameters for their racemization. The inversion demonstrates that the gold−thiolate interface is anything but fixed; in contrast, it is rather flexible. This result is of fundamental interest and needs to be considered in future applications.

A second line of our research is the selective introduction of chiral, bidentate ligands into the ligand layer of intrinsically chiral gold clusters. The ligand exchange reaction is highly diastereoselective. The bidentate ligand connects two of the protecting units on the cluster surface and thus effectively stabilizes the cluster against thermally induced inversion. A minor (but significant) influence of chiral ligands to the CD spectra of the clusters is observed. The studied system represents the first example of an intrinsically chiral gold cluster with a defined number of exchanged ligands, full control over their regio- and stereochemistry. The methodology allows for the selective preparation of mixed-ligand cluster compounds and a thorough investigation of the influence of single ligands on the cluster's properties. Overall, the method enables even more detailed tailoring of properties.

Still, central questions remain unanswered: (1) Is intrinsic chirality a ubiquitous feature of thiolate-protected gold clusters? (2) How does chirality transfer work? (3) What are the applications for chiral thiolate-protected gold clusters?

In this Account, we summarize the main findings on chirality in thiolate-protected gold cluster of the past half decade. Emphasis is put on intrinsically chiral clusters and their structures, optical activity, and reactivity.

1. INTRODUCTION

Thiolate-protected gold clusters (10−200 Au atoms) have recently aroused significant interest due to their molecular, strongly size-dependent behavior, stability, and tunability of properties.[1−4] It was observed that certain sizes show exceptional stability and are ubiquitous reaction products,[5,6] while others are only formed under special conditions. The formulation of the Superatom Complex Model (SACM) allows explaining their stability.[7−9] Unlike larger nanoparticles, monolayer-protected gold clusters do not exhibit a localized surface plasmon resonance (LSPR, Figure 1). Instead, featured absorption spectra are found.[10] This is ascribed to discrete energy levels in the clusters. The spectra cannot be predicted as a size-dependent function (whereas the size-dependent plasmon resonance can be modeled using Mie theory[11]). This is closely related to their structures.

The interface between the core of the cluster and the thiolate ligands consists of a bridged binding motif (Figure 2). A Au(I) atom is stabilized between the sulfur atoms of two neighboring ligands. This experimental finding was predicted ("divide-and-protect").[12] The binding motif can be thought as bidentate binding of short oligomers $SR(AuSR)_n$ (n = 1, 2) and was found in several crystal structures.[13−17] Furthermore, the motif was observed in scanning tunneling microscopy studies of self-assembled monolayers (SAMs) (ref 18; ref 1 and references therein).

Chirality is one of the most-studied phenomena in chemical sciences. Its ubiquitous presence in biological systems leads to strong demand for development of asymmetric drugs, sensors, and catalysts. It is also expected to play an important role in the development of metamaterials (e.g., ref 19). Chirality on the nanoscale has become an intensively investigated field in modern material sciences.[20] Intrinsic chirality in thiolate-protected gold clusters[13,16,21−25] has given rise to the assumption that these systems could play a pivotal role in applications of cluster-based materials. We herein highlight recent findings on intrinsically chiral thiolate-protected clusters.

Received: December 11, 2013
Published: March 3, 2014

   dx.doi.org/10.1021/ar400295d | *Acc. Chem. Res.* 2014, 47, 1318−1326

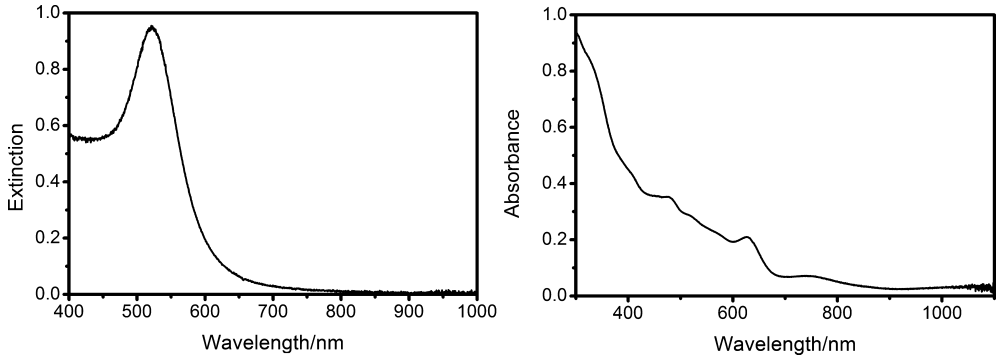

Figure 1. Left: UV−vis spectrum of a 20 nm sized citrate-stabilized gold nanoparticle. A strong LSPR is found. Right: UV−vis spectrum of $Au_{38}(SCH_2CH_2Ph)_{24}$ clusters. The spectrum shows several defined transitions. The strongly featured spectrum is due to distinct electronic transitions, in contrast to the collective electron oscillation in the 20 nm nanoparticle.

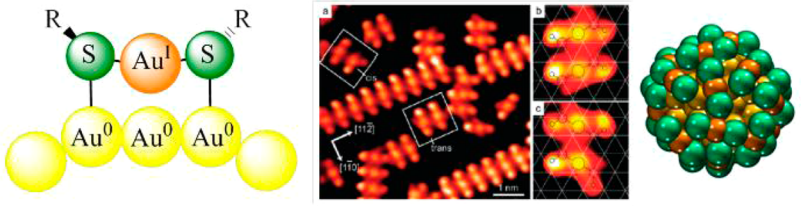

Figure 2. Protecting units in thiolate-protected gold clusters and on extended surfaces. Left: schematic of a (short) SR-Au-SR unit. Middle: STM image of methylthiolate on a Au(111) surface. Reprinted with permission from ref 18. Copyright 2009 American Chemical Society. Right: crystal structure of the $Au_{102}(p\text{-MBA})_{44}$ cluster (ref 13; the organic rest is not shown). The Au atoms in the schematics are colored according to their oxidation state.

2. CHIRALITY IN GOLD CLUSTERS

Thiolate-protected gold clusters can show chirality at different levels: (1) Protection with chiral thiolate ligands; (2) arrangement of the ligands on the surface of the cluster; (3) inherent chirality of the cluster core; and (4) *cis*/*trans* isomerism in the bridged Au−S binding motifs. Whereas the first way to bestow chirality to gold clusters is rather trivial and has been shown in numerous examples,[26−37] the other three features are much more sophisticated and complicated to assess experimentally. Inherently chiral cluster cores have been proposed as minimum energy geometries for various clusters.[38] It is found in bare metal clusters, for example, in Au_{34}^- and Au_{55} (Ag_{55} and Cu_{55} form regular icosahedra).[39−43] A similar distortion from a symmetric structure is found in the core of the $Au_{25}(SR)_{18}$ cluster.[44,45] However, these small distortions are probably difficult to be discriminated by chirally sensitive measurement techniques such as circular dichroism.

The bridged binding motifs $SR(AuSR)_n$ form semirings on the cluster surface, and the organic rests of the ligands can adopt *cis* and *trans* geometries (for n = 1). For near sp^3 hybridization, the sulfur atoms have four different substituents in tetrahedral coordination geometry. This renders them as stereogenic centers, and the absolute configuration can be assigned for the monomeric units SR-Au-SR (Scheme 1). The situation is more complicated in the dimeric units (n = 2). The central sulfur atom is either pseudochiral or its configuration is not readily assignable.

The *cis*/*trans* isomerism of the protecting units is difficult to assess experimentally. Computations showed the influence of the orientation of the ligands with respect to the units, leading to different energy and CD spectra.[46,47] This can lead to (weak) optical activity in structures, in which no "locked" stereogenic elements are found. Of note, the absolute configuration of the sulfur atoms can lead to 2^{18} = 262 144 and 2^{24} = 16 777 216 different stereoisomers in $Au_{25}(SR)_{18}$ and $Au_{38}(SR)_{24}$, respectively. While some of these configurations may lead to redundant structures, a vast number of isomers remains and finding the isomer of minimum energy is difficult.

Scheme 1. Stereochemistry in Protecting Units on the Surface of Gold Clusters[a]

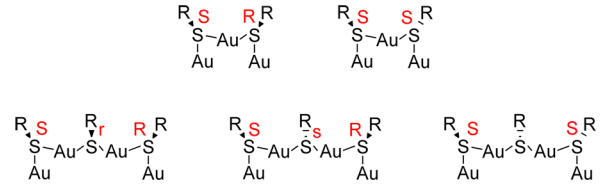

[a]The gold atoms at the bottom of the structures are Au(0) atoms at the surface of the cluster core, while the gold atoms stabilized between two sulfur atoms are formal Au(I). The stereodescriptors are indicated in red, and lowercase indicates pseudochirality. Priority for the determination of absolute configuration is Au(0) > Au(I) > R > electron lone pair.

3. CRYSTAL STRUCTURES OF THIOLATE-PROTECTED GOLD CLUSTERS

3.1. $Au_{102}(p\text{-MBA})_{44}$

A milestone in the field was the successful determination of the crystal structure of $Au_{102}(p\text{-MBA})_{44}$ (Figure 3A).[13] The core can be thought of as a 49-atom Marks decahedron and additional 30 surface atoms split into two 15-atom-subgroups on opposite sites. Fivefold symmetry is found for the core of the cluster, in which 19 short and two long units $SR(AuSR)_x$ (x = 1, 2) protect the core.

dx.doi.org/10.1021/ar400295d | *Acc. Chem. Res.* 2014, 47, 1318−1326

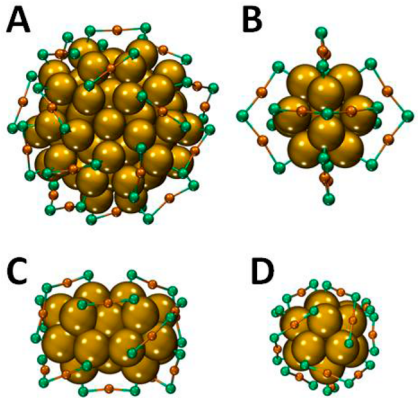

Figure 3. Crystal structure of the $Au_{102}(p\text{-MBA})_{44}$ cluster (A), $Au_{25}(2\text{-PET})_{18}$ (B), and $Au_{38}(2\text{-PET})_{24}$ in side-view (C) and along its principal axis (D). For the latter, the left-handed *A*-enantiomer is shown. The organic groups are removed. Atomic positions are from refs 13, 14, and 16. Yellow, Au_{Core}; orange, Au_{Adatom}; green, sulfur.

3.2. $Au_{38}(2\text{-PET})_{24}$

The structure of $Au_{38}(2\text{-PET})_{24}$ (2-PET: 2-phenylethylthiolate) was solved in 2010 (Figure 3C/D).[16] A correct prediction of its intrinsic chirality was made by Lopez-Acevedo et al.,[46] while the basic structural features were proposed by Zeng et al.[48] The cluster consists of a face-fused bi-icosahedral Au_{23} core which is protected by six dimeric and three monomeric units. The short units are arranged along the equator of the prolate core and the long units form two triblade fans at its ends. The fans have the same handedness, giving rise to chirality. We propose the use of the descriptors *C* and *A* (clockwise/anticlockwise) for the right- and left-handed enantiomers. Strictly, the cluster should be labeled as *A,A*- or *C,C*-$Au_{38}(SR)_{24}$, since the structure proposed by Zeng et al. has opposite handedness for the two fans (*A,C*-$Au_{38}(SR)_{24}$). We will make this distinction only when necessary.

3.3. $Au_{25}(2\text{-PET})_{18}$

The crystal structure of $Au_{25}(2\text{-PET})_{18}$ consists of a Au_{13} core with six dimeric units (Figure 3B).[14] A slight distortion is found in both the anionic and neutral form.[15] These distortions mainly affect the protecting units, which are flexible. It seems unlikely, that one can discriminate these (chiral) distortions experimentally.

3.4. $Au_{28}(TBBT)_{20}$

The structure of $Au_{28}(TBBT)_{20}$ (TBBT: *p*-tertbutylbenzenethiol) consists of a Au_{14} core protected by four dimeric and two trimeric ($Au_3(SR)_4$) units.[23,49] The dimeric units form two subsets of two units each, which are arranged in a chiral fashion.

The intrinsic chirality of thiolate-protected gold clusters is a unique feature that arises from the "divide-and-protect"-type gold−thiolate interface. The protecting units arrange on the curved surface of the cluster core in a two-point interaction. This has two important consequences: (1) the units arrange in a fashion that minimizes the steric interaction between the units and organic rests of the ligands (we ignore stabilizing interactions between the ligands here and refer solely to steric demand). Considering $Au_{38}(SR)_{24}$, this becomes obvious when comparing the *A,C*-isomer and the more stable *A,A*- or *C,C*-structure. The distances between the sulfur atoms in the monomeric units at the "equator" of the core and the nearest sulfur atom of a neighboring dimeric unit (central sulfur atom) are considerably longer in the chiral than in the achiral structure (average 4.606 vs 4.171 Å). This leads to stronger steric hindrance between the organic rests of the thiolates in the achiral isomer (Figure 4). The prolate nature of the $Au_{38}(SR)_{24}$ cluster allows for the dimer units to arrange in helical fashions and adopt to the interaction with the monomeric units. (2) The two-point interaction between the protecting units and the cluster core prevents the ligands from free rotation. As discussed below, the enantiomers of intrinsically chiral clusters such as $Au_{38}(SR)_{24}$ are stable at room temperature.

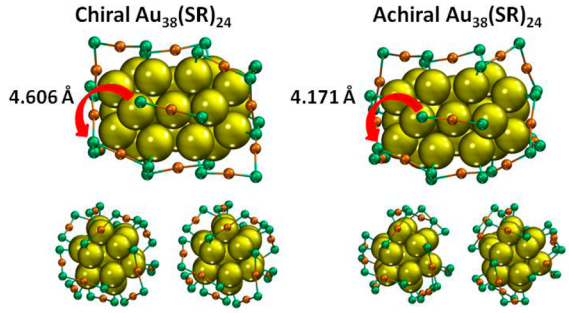

Figure 4. Top: Chiral (left) and achiral (right) structures of $Au_{38}(SR)_{24}$ in comparison (coordinates from ref 46). Marked with arrows are one sulfur atom of one monomeric unit and the nearest sulfur atom from a neighboring dimeric unit. The average distances over the cluster are assigned. Bottom: Views along the principal axis of the isomers in both directions. The chiral structure shows the same handedness; the achiral structure shows opposite handedness.

4. OPTICAL ACTIVITY IN THIOLATE-PROTECTED GOLD CLUSTERS

4.1. Gold Clusters Protected with Chiral Thiolates

Chiral protecting ligands lead to significant Cotton effects in the visible range of the electromagnetic spectrum and gives rise to strong circular dichroism responses. This has first been demonstrated by Whetten and co-workers.[26] Several ligands have been used to study the optical activity of gold clusters, and numerous examples focused on cysteine-derived ligands.[27−30,50,51] The $Au_{25}(SR)_{18}$ cluster has been extensively studied and was prepared with different chiral ligands.[26,34,35,37] The CD spectra give insight into the influence of a ligand on the optical activity. The absorption spectra of the cluster protected with *L*-glutathionate,[26] 1-methyl-2-phenylethylthiolate (pet*),[34] camphorthiolate (CamS),[37] and captopril (Capt)[35] are very similar, but the CD spectra reveal an interesting observation: All clusters, except for pet*-protected ones, show similar CD spectra. Given the fact that pet* is the least bulky ligand, it has been speculated that it induces a different *cis/trans* configuration in the protecting units, which may alter the shape of the CD spectrum.[37] Experimental proof of this interpretation is lacking, however.

4.2. Intrinsically Chiral Gold Clusters

The successful determination of the structures of $Au_{102}(p\text{-MBA})_{44}$ and $Au_{38}(2\text{-PET})_{24}$ stimulated the search for a way to resolve the enantiomers of the clusters.[13,16] Chiral High-Performance Liquid Chromatography (HPLC) was found to be an effective method for the enantioseparation of $Au_{38}(2\text{-PET})_{24}$.[21,52] The CD spectra of the enantiomers are perfect mirror images and the CD spectrum of the enantiomer eluting last from the HPLC column is in very good agreement with a computed spectrum of a right-handed model cluster, *C*-

dx.doi.org/10.1021/ar400295d | Acc. Chem. Res. 2014, 47, 1318−1326

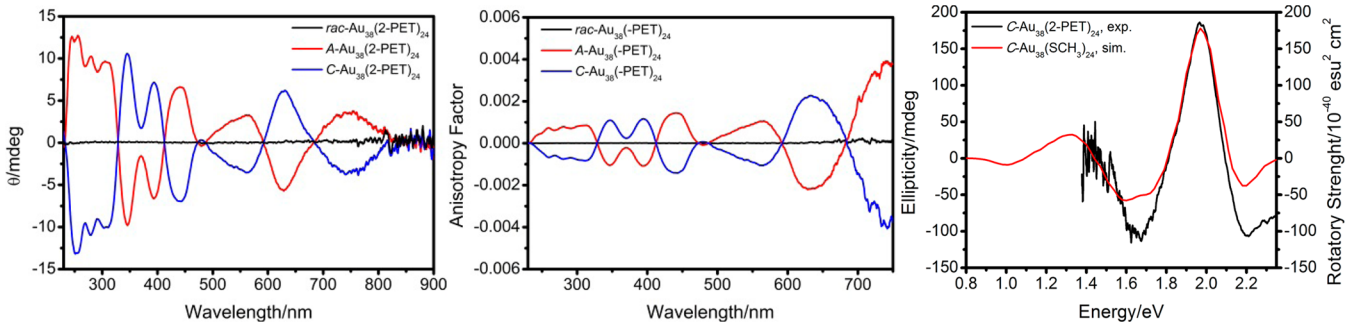

Figure 5. CD spectra (left) and anisotropy factors (middle) of $Au_{38}(2\text{-PET})_{24}$ clusters after enantioseparation. Right: Comparison between the experimental CD spectrum of the enantiomer eluting last from the column and calculations for *C*-$Au_{38}(SCH_3)_{24}$. The good match allows assignment of handedness. The data were originally published in refs 21 and 46.

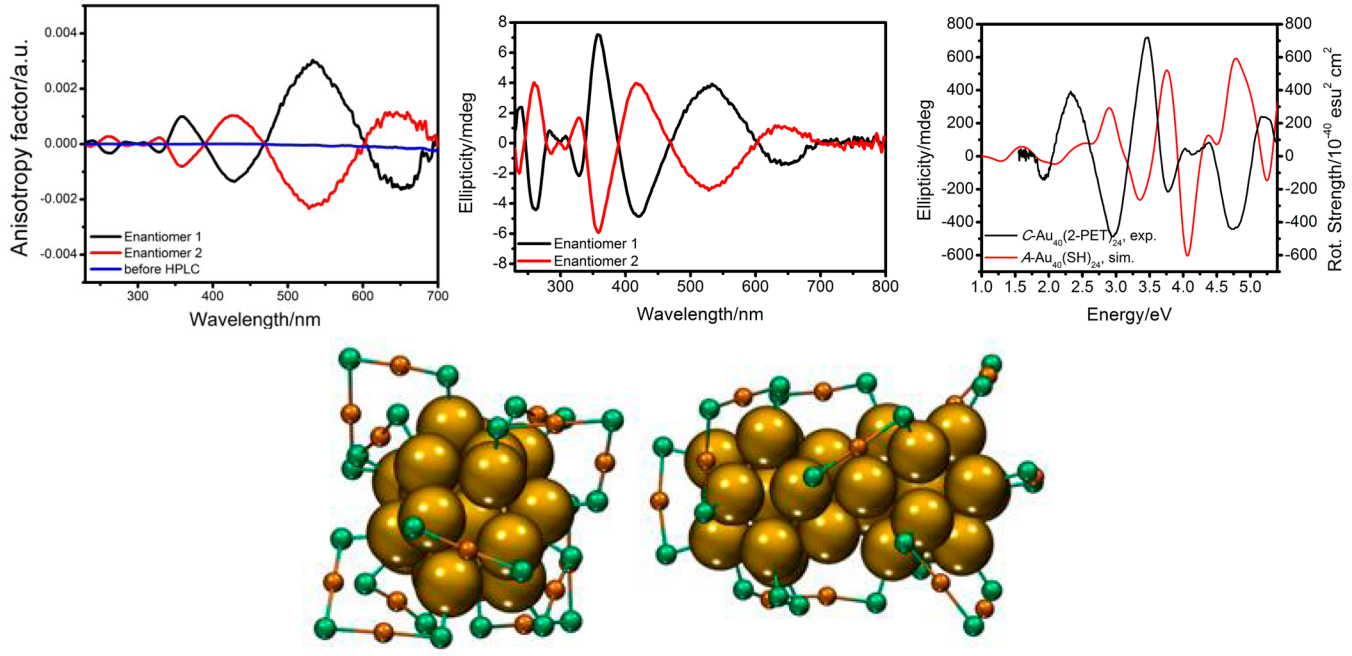

Figure 6. Top: Anisotropy factors (left) and CD spectra of $Au_{40}(2\text{-PET})_{24}$ (middle), comparison between the measured and calculated CD spectrum of $Au_{40}(2\text{-PET})_{24}$ (right). For the comparison, the spectra were plotted as "enantiomers" in order to highlight the match. The calculated spectrum is the one of *A*-$Au_{40}(SH)_{24}$; accordingly, "enantiomer 1" corresponds to *C*-$Au_{40}(2\text{-PET})_{24}$. Bottom: Proposed structure of the right-handed $Au_{40}(SR)_{24}$ cluster. Data and coordinates are from refs 22 and 47. Yellow, Au_{Core}; orange, Au_{Adatom}; green, sulfur.

$Au_{38}(SMe)_{24}$ (Figure 5).[46] Therefore, assignment of the handedness is possible (which CD spectroscopy alone does not readily provide).

Similarly, $Au_{40}(2\text{-PET})_{24}$ clusters were enantioenriched via HPLC and the collected fractions show strong optical activity with mirror-image relationship (Figure 6, top).[22,53] As yet, the crystal structure of $Au_{40}(SR)_{24}$ is not available, but the results suggest intrinsic chirality similar to that found in Au_{38} and Au_{102}. A structural model was proposed in a DFT study (Figure 6, bottom).[47] The cluster is proposed to consist of a Au_{26} core protected with six mono- and four dimeric protecting units. The core is composed of two icosahedrons in edge-to-edge contact and rotation of 90°. Four monomeric units are arranged along the "equator" of the cluster core and the ends of the "nanorod" are capped with two sets consisting of two dimeric and one monomeric unit. The units are arranged in a staggered fashion very similar to $Au_{38}(SR)_{24}$. A fair agreement between simulated and experimental absorption and CD spectra was found, which allows assignment of handedness.[47] A different structure with a Au_{23} core was predicted to have very similar energies, but, as yet, no optical properties are available.[9] The enantiomers of $Au_{28}(TBBT)_{20}$ were separated by HPLC and CD spectra were recorded.[23] As in $Au_{40}(SR)_{24}$, a series of electronic transitions is resolved in the CD spectrum that is not found in the UV−vis spectrum. Computations allow assignment of handedness of the cluster by comparison of measured to simulated CD spectra.[49]

Both $Au_{38}(2\text{-PET})_{24}$ and $Au_{40}(2\text{-PET})_{24}$ show strong optical activity with maximum anisotropy factors in the range of 5×10^{-3},[21,22,53] which exceed the typical anisotropy factors of clusters protected with chiral thiolates.[54] Even the $Au_{38}(L\text{-SG})_{24}$ cluster shows weaker optical activity,[27] although one might expect cooperative effects between the chiral ligand and the chiral cluster. Comparison of the CD spectra of $Au_{38}(2\text{-PET})_{24}$ and $Au_{38}(L\text{-SG})_{24}$ shows very similar curves,[21] indicating that one enantiomer (the right-handed one) of the cluster is formed under the influence of the chiral *L*-glutathione. Overall, comparison of the CD spectra of $Au_{38}(SR)_{24}$ indicates

dx.doi.org/10.1021/ar400295d | Acc. Chem. Res. 2014, 47, 1318−1326

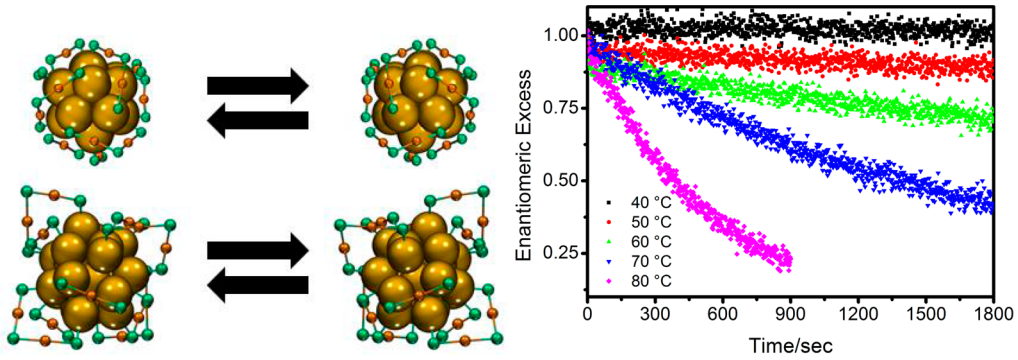

Figure 7. Left: Inversion reaction of $Au_{38}(SR)_{24}$ (top) and $Au_{40}(SR)_{24}$ (bottom). Right: Evolution of the enantiomeric excess of $Au_{38}(2\text{-PET})_{24}$ at different temperatures. Acceleration of the racemization is observed for higher temperatures. Data were originally published in ref 52.

a rather low influence of the ligand. Additional evidence of selective formation of one handedness of the cluster under the influence of enantiopure thiolates is provided by experiments conducted with *R*- and *S*-pet* and captopril.[55] Note that calculations predict that even smaller thiolate-protected gold clusters than those discussed above can be chiral.[56]

4.3. Inversion of Intrinsically Chiral Gold Clusters

The fact that the enantiomers of $Au_{38}(SR)_{24}$ and $Au_{40}(SR)_{24}$ are stable at room temperature suggests a sufficiently high racemization barrier. This barrier was determined for $Au_{38}(2\text{-PET})_{24}$ and $Au_{40}(2\text{-PET})_{24}$.[52,53] An enantiopure solution of the clusters is heated to different temperatures and the optical activity is followed with time (Figure 7). The strength of the CD response is a function of the enantiomeric excess of the sample. HPLC control experiments showed no hints for decomposition of the clusters.

Racemization proceeds with first-order kinetics and the activation barrier was determined to be in the range of 29 kcal/mol. This value is low compared to typical energies of Au−S bonds (ca. 50 − 60 kcal/mol), but is in the range of the chemisorption enthalpies of thiols and disulfides in the formation of SAMs.[57−62] A similar activation energy is found for $Au_{40}(2\text{-PET})_{24}$ (24 kcal/mol), but a negative entropy of activation is observed.[53] This suggests a different pathway for the inversion of the cluster. Therefore, higher temperatures are needed to induce the racemization of $Au_{40}(2\text{-PET})_{24}$. The inversion of $Au_{38}(2\text{-PET})_{24}$ is effectively hindered by introducing one bidentate ligand (see below).[63] While the activation energies for inversion are very similar in all cases, it was observed that the entropy of activation varies significantly.

Mechanisms for the inversion of $Au_{38}(SR)_{24}$ and $Au_{40}(2\text{-PET})_{24}$ were proposed,[52,53] but experimental insights into these are lacking. While the elucidation of the mechanism desires more detailed work, the flexibility of the Au-thiolate interface in thiolate-protected gold clusters was demonstrated using the inherent chirality and circular dichroism as a probe. The fact that rearrangement of the ligand layer on the surface of a gold cluster is feasible should be considered in future applications that require rather drastic conditions (e.g., elevated temperatures).

5. LIGAND EXCHANGE REACTIONS INTRODUCING CHIRAL LIGANDS

In ligand exchange reactions, a cluster $Au_m(SR)_n$ is reacted with an excess of incoming ligand HSR′. This forms a mixture of clusters with different compositions $Au_m(SR)_{n-x}(SR')_x$ (x = 0−n).[36,64−74] If chiral ligands are involved, the CD response is a superposition of the individual CD spectra of the different ligand compositions in the product.[33,36,68,75] Introduction of chiral ligands leads to increasing optical activity until the reaction is equilibrated.

Comparison of the evolution of optical activity with the extent of exchange gives useful insight into the contribution of individual ligands on the CD spectra of the clusters. The reaction of $Au_{38}(2\text{-PET})_{24}$ and $Au_{40}(2\text{-PET})_{24}$ with bidentate 1,1′-binaphthyl-2,2′-dithiol (BINAS, Scheme 2) was found to be slow and BINAS binds in a bidentate fashion. Even at very low BINAS-coverage of the clusters, strong optical activity is induced.[36,68]

Scheme 2. Structure of 1,1′-Binaphthyl-2,2′-dithiol

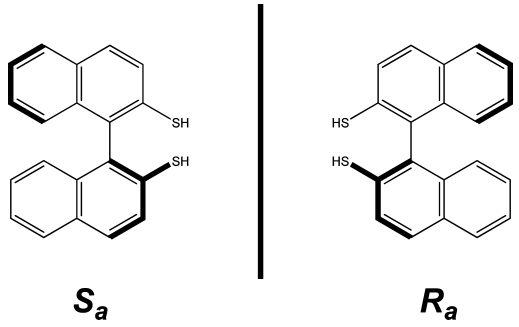

Starting from a chiral, but racemic, cluster, the evolving CD spectra are a superposition of the individual CD spectra of the enantiomers (which did not react) and diastereomeric exchange products. If only one chiral ligand is present, the reaction product then consists of the two enantiomers (unexchanged clusters) and two diastereomers (exchanged clusters). For the diastereomers, the handedness of the chiral ligand is the same, but the handedness of the cluster is different. Overall, four chiral species are found. Assuming that the place-exchange reaction is *not diastereoselective*, the starting enantiomers react at the *same rate*; their CD spectra cancel and do not contribute to the net optical activity. The measured CD spectrum is the difference between the CD spectra of the diastereomers. This should result in rather weak optical activity. If the ligand exchange reaction has *different rate* constants for the two enantiomers (*diastereoselective*), unequal amounts of the enantiomers of the unreacted cluster and the reaction products are expected. The CD spectra of the four species overlay in this case.

dx.doi.org/10.1021/ar400295d | *Acc. Chem. Res.* 2014, 47, 1318−1326

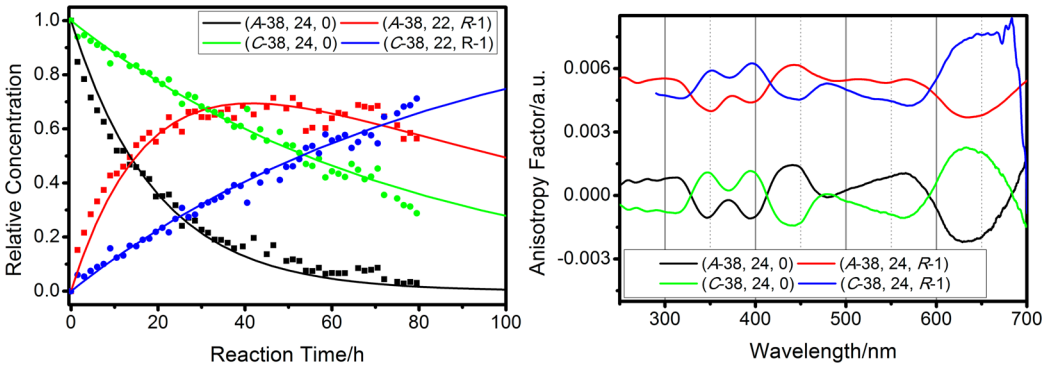

Figure 8. Left: Concentration profiles of the ligand exchange reaction of *A*- and *C*-$Au_{38}(2\text{-PET})_{24}$ (black and green) with *R*-BINAS. The left-handed cluster reacts much faster than the right-handed enantiomer. Right: Anisotropy factors of $Au_{38}(2\text{-PET})_{24}$ and $Au_{38}(2\text{-PET})_{22}(R\text{-BINAS})_1$. The spectra of the diastereomers (red and blue) resemble those of the unsubstituted enantiomers (black, green). Data were originally published in refs 63 and 76.

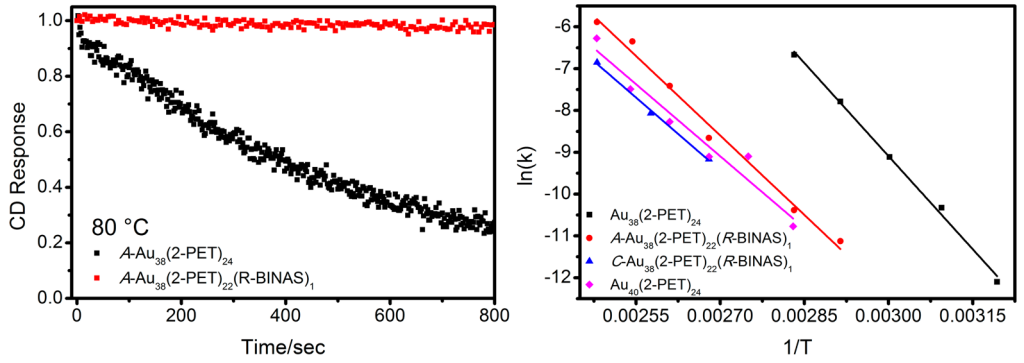

Figure 9. Left: Normalized optical activity of $Au_{38}(2\text{-PET})_{24}$ and *A*-$Au_{38}(2\text{-PET})_{22}(R\text{-BINAS})_1$ at 80 °C. While the unsubstituted cluster shows fast decrease of optical activity (black), BINAS-substitution leads to almost constant values (red). Right: Arrhenius plots for $Au_{38}(2\text{-PET})_{24}$ (black), *A*-$Au_{38}(2\text{-PET})_{22}(R\text{-BINAS})_1$ (red), *C*-$Au_{38}(2\text{-PET})_{22}(R\text{-BINAS})_1$ (blue), and $Au_{40}(2\text{-PET})_{24}$ (magenta). The data were originally published in refs 52, 63, and 53.

Table 1. Activation Parameters for the Thermal Inversion of $Au_{38}(2\text{-PET})_{24}$, *A*-$Au_{38}(2\text{-PET})_{22}(R\text{-BINAS})_1$, and *C*-$Au_{38}(2\text{-PET})_{22}(R\text{-BINAS})_1$

	E_a (kcal·mol^{-1})	$\Delta H^{\ddagger}$ (kcal·mol^{-1})	$\Delta S^{\ddagger}$ (cal·mol^{-1}·K^{-1})	$\Delta G^{\ddagger}$ (kcal·mol^{-1})
$Au_{38}(2\text{-PET})_{24}$	29.5	28.8	9.7	25.6
$Au_{40}(2\text{-PET})_{24}$	25.0	24.4	−12.0	28.8
A-$Au_{38}(2\text{-PET})_{22}(R\text{-BINAS})_1$	25.2	24.4	−10.1	28.2
C-$Au_{38}(2\text{-PET})_{22}(R\text{-BINAS})_1$	23.0	22.3	−17.6	29.1

For the well-characterized $Au_{38}(SR)_{24}$ cluster, HPLC experiments were performed to study the reaction with enantiopure *R*-BINAS in situ.[76] A clear difference in the reaction rates of the enantiomers of $Au_{38}(2\text{-PET})_{24}$ was observed when the cluster reacted with *R*-BINAS and it was found that *R*-BINAS has a preference for *A*-$Au_{38}(2\text{-PET})_{24}$ (Figure 8, left). Furthermore, it was found that the second exchange step is much slower than the first exchange. We isolated the diastereomeric reaction products *A*-$Au_{38}(2\text{-PET})_{22}(R\text{-BINAS})_1$ and *C*-$Au_{38}(2\text{-PET})_{22}(R\text{-BINAS})_1$.[63] This approach yields pure, mixed-ligand clusters with a defined number of exchanged ligands. The optical properties of $Au_{38}(SR)_{24}$ are affected by the BINAS ligand in a minor way. Similarly, the CD spectra of the diastereomeric clusters bear resemblance to those of the parent enantiomers, allowing assignment of the handedness of the cluster (Figure 8, right).

We compared the activation barriers of inversion of BINAS-functionalized Au_{38} clusters to those of $Au_{38}(2\text{-PET})_{24}$. Significantly higher temperatures are needed to induce a change in optical activity, hence the inversion is hindered (Figure 9, left). It was found that the activation energy is lower than in $Au_{38}(2\text{-PET})_{24}$ and the entropy of activation changes from positive to negative values after BINAS-substitution, which affects the Gibbs enthalpy of activation (Figure 9, right and Table 1). This gives rise to the assumption that a different pathway is followed. The results clearly indicate that BINAS-substitution leads to enhanced stability of the $Au_{38}(SR)_{24}$ cluster against inversion.

The fact that a different inversion pathway is likely in BINAS-substituted clusters raises the question of the binding site of the bidentate ligand. It has long been assumed that BINAS preferentially binds to the monomeric protecting units.[33,36,68,76] This interpretation was challenged by a MALDI study on the ligand exchange between $Au_{25}(2\text{-PET})_{18}$ and BINAS. Au_{25} is protected by dimeric units only and survives the exchange without decomposition.[77] Based on this, a very recent DFT study revealed interunit binding of BINAS between two dimeric units in $Au_{38}(SR)_{24}$ (Figure 10).[78] This model is consistent

dx.doi.org/10.1021/ar400295d | Acc. Chem. Res. 2014, 47, 1318−1326

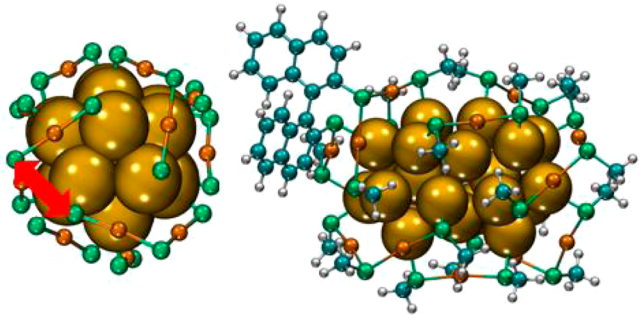

Figure 10. Optimized structure of *A*-$Au_{38}(2\text{-PET})_{22}(R\text{-BINAS})_1$. Left: $Au_{38}(2\text{-PET})_{24}$ along its (idealized) C_3 axis. Binding sites of BINAS are highlighted by the red arrow. Right: Au_{38} cluster with the BINAS ligand (side view). Coordinates are from ref 78. Yellow, Au_{Core}; orange, Au_{Adatom}; green, sulfur; blue, carbon; white, hydrogen.

with studies on bidentate ligands on $Au_{25}(SR)_{18}$.[66,67] The increased stability of the $Au_{38}(SR)_{22}(BINAS)_1$ clusters against thermally induced inversion may be explained by the bridging of the units by the BINAS ligand.[63] Since the dimeric units are involved in this inversion, the binding site of the ligand has paramount importance and forces the cluster to follow a different pathway during inversion. It should be noted that a monodentate ligand can change its binding site when heating the cluster.[79]

6. CONCLUSION AND OUTLOOK

Recent efforts toward understanding chiral thiolate-protected gold clusters have seen significant advances which revealed interesting properties. Chirality can be induced to clusters by the use of chiral thiolate ligands or is found as an intrinsic property of the clusters. For the latter, no chiral ligands are required, but synthesis yields racemic mixtures. The separation of enantiomers was demonstrated with chiral HPLC. The optical activity of such intrinsically chiral clusters is strong. Thermal inversion experiments revealed significant flexibility of the gold−sulfur interface.

Ligand exchange experiments with bidentate BINAS show diastereoselectivity when a racemic mixture is used. Diastereomeric clusters *A*-or *C*-$Au_m(SR)_{n-x}(SR^*)_x$ can be isolated using HPLC, yielding very defined species, in the case of $Au_{38}(2\text{-PET})_{22}(BINAS)_1$ even with regioselectivity. The interunit binding motif in the BINAS-case stabilizes the cluster against inversion.

Future studies should be devoted to testing chiral clusters in catalysis or sensing applications. The flexibility of the Au-thiolate interface is a substantial property that deserves further insight since it has to be considered in applications.

In summary, the recent work may allow quantification of contribution of the individual levels of chirality (distorted cores, *cis*/*trans* isomerism at sulfur atoms, arrangement of protecting units, chiral ligands) on the optical activity. Adsorption site studies (e.g., the successful determination of the crystal structure) on mixed-ligand protected clusters may allow selective manipulation of cluster properties for specific purposes. Chirality and CD spectroscopy have been proven as a useful tool to assess these properties experimentally and theoretically. The paramount importance of chirality for catalytic and biologic applications is an additional motivation.

AUTHOR INFORMATION

Corresponding Authors

*E-mail: stefan.knoppe@chem.kuleuven.be.
*E-mail: Thomas.Bürgi@unige.ch.

Present Address

†S.K.: Molecular Imaging and Photonics, Department of Chemistry, KU Leuven, Celestijnenlaan 200D, 3001 Heverlee, Belgium.

Notes

The authors declare no competing financial interest.

Biographies

Stefan Knoppe studied chemistry at the Universities of Kiel and Heidelberg (Germany) where he obtained his diploma (2009). He obtained a Ph.D. from the University of Geneva (2012) and currently is a postdoctoral fellow of the German Academic Exchange Service at KU Leuven (Belgium), where he studies chiral and magnetic nanoparticles.

Thomas Bürgi studied chemistry and obtained his Ph.D. (1995) at the University of Berne (Switzerland). After a postdoc at MIT, he did his habilitation at ETH, Zürich. He became assistant professor at the University of Neuchâtel (Switzerland, 2005) and full professor at the University of Heidelberg (2008). In 2010, he moved to the University of Geneva, where he is professor of physical chemistry. His research focuses on chiral nanoparticles, plasmon-based metamaterials and in situ vibrational spectroscopy.

ACKNOWLEDGMENTS

This work was supported by the University of Geneva and the Swiss National Science Foundation. We would like to thank all co-workers and collaborators for their support. Notable contributions were made by Igor Dolamic, Birte Varnholt, Raymond Azoulay, Sophie Michalet (University of Geneva), Amala Dass (University of Mississippi), Hannu Häkkinen (University of Jyväskylä, Finland), and Richard Palmer (University of Birmingham, UK). We thank O. Lopez-Acevedo (Aalto University, Finland) for providing the simulated CD spectrum of *C*-$Au_{38}(SCH_3)_{24}$.

REFERENCES

(1) Häkkinen, H. The gold-sulfur interface at the nanoscale. *Nat. Chem.* **2012**, *4*, 443−455.
(2) Qian, H.; Zhu, M.; Wu, Z.; Jin, R. Quantum sized gold nanoclusters with atomic precision. *Acc. Chem. Res.* **2012**, *45*, 1470−1479.
(3) Jin, R. Quantum sized, thiolate-protected gold nanoclusters. *Nanoscale* **2010**, *1*, 343−362.
(4) Aikens, C. M. Electronic Structure of Ligand-Passivated Gold and Silver Nanoclusters. *J. Phys. Chem. Lett.* **2011**, *2*, 99−104.
(5) Negishi, Y.; Takasugi, Y.; Sato, S.; Yao, H.; Kimura, K.; Tsukuda, T. Magic-numbered Au_n clusters protected by glutathione monolayers (n = 18, 21, 25, 28, 32, 39): Isolation and spectroscopic characterization. *J. Am. Chem. Soc.* **2004**, *126*, 6518−6519.
(6) Negishi, Y.; Nobusada, K.; Tsukuda, T. Glutathione-protected gold clusters revisited: Bridging the gap between gold(I)-thiolate complexes and thiolate-protected gold nanocrystals. *J. Am. Chem. Soc.* **2005**, *127*, 5261−5270.
(7) Walter, M.; Akola, J.; Lopez-Acevedo, O.; Jadzinsky, P. D.; Calero, G.; Ackerson, C. J.; Whetten, R. L.; Grönbeck, H.; Häkkinen, H. A unified view of ligand-protected gold clusters as superatom complexes. *Proc. Natl. Acad. Sci. U.S.A.* **2008**, *105*, 9157−9162.

(8) Pei, Y.; Zeng, X. C. Investigating the structural evolution of thiolate protected gold clusters from first-principles. *Nanoscale* **2012**, *4*, 4054−4072.
(9) Jiang, D. E. The expanding universe of thiolated gold nanoclusters and beyond. *Nanoscale* **2013**, *5*, 7149−7160.
(10) Wyrwas, R. B.; Alvarez, M. M.; Khoury, J. T.; Price, R. C.; Schaaff, T. G.; Whetten, R. L. The colours of nanometric gold - Optical response functions of selected gold-cluster thiolates. *Eur. Phys. J. D* **2007**, *43*, 91−95.
(11) Mie, G. Beiträge zur Optik trüber Medien, speziell kolloidaler Metallösungen. *Ann. Phys.* **1908**, *330*, 377−445.
(12) Häkkinen, H.; Walter, M.; Grönbeck, H. Divide and protect: Capping gold nanoclusters with molecular gold-thiolate rings. *J. Phys. Chem. B* **2006**, *110*, 9927−9931.
(13) Jadzinsky, P. D.; Calero, G.; Ackerson, C. J.; Bushnell, D. A.; Kornberg, R. D. Structure of a thiol monolayer-protected gold nanoparticle at 1.1 A resolution. *Science* **2007**, *318*, 430−433.
(14) Heaven, M. W.; Dass, A.; White, P. S.; Holt, K. M.; Murray, R. W. Crystal structure of the gold nanoparticle $[N(C_8H_{17})_4][Au_{25}(SCH_2CH_2Ph)_{18}]$. *J. Am. Chem. Soc.* **2008**, *130*, 3754−3755.
(15) Zhu, M.; Eckenhoff, W. T.; Pintauer, T.; Jin, R. Conversion of Anionic $[Au_{25}(SCH_2CH_2Ph)_{18}]^-$ Cluster to Charge Neutral Cluster via Air Oxidation. *J. Phys. Chem. C* **2008**, *112*, 14221−14224.
(16) Qian, H.; Eckenhoff, W. T.; Zhu, Y.; Pintauer, T.; Jin, R. Total structure determination of thiolate-protected Au_{38} nanoparticles. *J. Am. Chem. Soc.* **2010**, *132*, 8280−8281.
(17) Zeng, C.; Qian, H.; Li, T.; Li, G.; Rosi, N. L.; Yoon, B.; Barnett, R. N.; Whetten, R. L.; Landman, U.; Jin, R. Total Structure and Electronic Properties of the Gold Nanocrystal $Au_{36}(SR)_{24}$. *Angew. Chem., Int. Ed.* **2012**, *51*, 13114−13118.
(18) Voznyy, O.; Dubowski, J. J.; Yates, J. T.; Maksymovych, P. The role of gold adatoms and stereochemistry in self-assembly of methylthiolate on Au(111). *J. Am. Chem. Soc.* **2009**, *131*, 12989−12993.
(19) Helgert, C.; Pshenay-Severin, E.; Falkner, M.; Menzel, C.; Rockstuhl, C.; Kley, E. B.; Tunnermann, A.; Lederer, F.; Pertsch, T. Chiral metamaterial composed of three-dimensional plasmonic nanostructures. *Nano Lett.* **2011**, *11*, 4400−4404.
(20) Wang, Y.; Xu, J.; Wang, Y.; Chen, H. Emerging chirality in nanoscience. *Chem. Soc. Rev.* **2013**, *42*, 2930−2962.
(21) Dolamic, I.; Knoppe, S.; Dass, A.; Bürgi, T. First enantioseparation and circular dichroism spectra of Au_{38} clusters protected by achiral ligands. *Nat. Commun.* **2012**, *3*, 798.
(22) Knoppe, S.; Dolamic, I.; Dass, A.; Bürgi, T. Separation of Enantiomers and CD Spectra of $Au_{40}(SCH_2CH_2Ph)_{24}$: Spectroscopic Evidence for Intrinsic Chirality. *Angew. Chem., Int. Ed.* **2012**, *51*, 7589−7591.
(23) Zeng, C.; Li, T.; Das, A.; Rosi, N. L.; Jin, R. Chiral Structure of Thiolate-Protected 28-Gold-Atom Nanocluster Determined by X-ray Crystallography. *J. Am. Chem. Soc.* **2013**, *135*, 10011−10013.
(24) Pei, Y.; Lin, S.; Su, J.; Liu, C. Structure Prediction of $Au_{44}(SR)_{28}$: A Chiral Superatom Cluster. *J. Am. Chem. Soc.* **2013**, *135*, 19060−19063.
(25) Tlahuice-Flores, A.; Jose-Yacaman, M.; Whetten, R. L. On the structure of the thiolated Au_{15} cluster. *Phys. Chem. Chem. Phys.* **2013**, *15*, 19557−19560.
(26) Schaaff, T. G.; Knight, G.; Shafigullin, M. N.; Borkman, R. F.; Whetten, R. L. Isolation and selected properties of a 10.4 kDa Gold: Glutathione cluster compound. *J. Phys. Chem. B* **1998**, *102*, 10643−10646.
(27) Schaaff, T. G.; Whetten, R. L. Giant gold-glutathione cluster compounds: Intense optical activity in metal-based transitions. *J. Phys. Chem. B* **2000**, *104*, 2630−2641.
(28) Yao, H.; Miki, K.; Nishida, N.; Sasaki, A.; Kimura, K. Large optical activity of gold nanocluster enantiomers induced by a pair of optically active penicillamines. *J. Am. Chem. Soc.* **2005**, *127*, 15536−15543.
(29) Yao, H.; Fukui, T.; Kimura, K. Chiroptical responses of D-/L-penicillamine-capped gold clusters under perturbations of temperature change and phase transfer. *J. Phys. Chem. C* **2007**, *111*, 14968−14976.
(30) Gautier, C.; Bürgi, T. Vibrational circular dichroism of *N*-acetyl-L-cysteine protected gold nanoparticles. *Chem. Commun.* **2005**, 5393−5395.
(31) Gautier, C.; Bürgi, T. Chiral N-isobutyryl-cysteine protected gold nanoparticles: preparation, size selection, and optical activity in the UV-vis and infrared. *J. Am. Chem. Soc.* **2006**, *128*, 11079−11087.
(32) Gautier, C.; Taras, R.; Gladiali, S.; Bürgi, T. Chiral 1,1′-binaphthyl-2,2′-dithiol-stabilized gold clusters: size separation and optical activity in the UV-vis. *Chirality* **2008**, *20*, 486−493.
(33) Si, S.; Gautier, C.; Boudon, J.; Taras, R.; Gladiali, S.; Bürgi, T. Ligand Exchange on Au_{25} Cluster with Chiral Thiols. *J. Phys. Chem. C* **2009**, *113*, 12966−12969.
(34) Zhu, M.; Qian, H.; Meng, X.; Jin, S.; Wu, Z.; Jin, R. Chiral Au nanospheres and nanorods: synthesis and insight into the origin of chirality. *Nano Lett* **2011**, *11*, 3963−3969.
(35) Kumar, S.; Jin, R. Water-soluble $Au_{25}(Capt)_{18}$ nanoclusters: synthesis, thermal stability, and optical properties. *Nanoscale* **2012**, *4*, 4222−4227.
(36) Knoppe, S.; Dharmaratne, A. C.; Schreiner, E.; Dass, A.; Bürgi, T. Ligand exchange reactions on Au_{38} and Au_{40} clusters: a combined circular dichroism and mass spectrometry study. *J. Am. Chem. Soc.* **2010**, *132*, 16783−16789.
(37) Knoppe, S.; Kothalawala, N.; Jupally, V. R.; Dass, A.; Bürgi, T. Ligand dependence of the synthetic approach and chiroptical properties of a magic cluster protected with a bicyclic chiral thiolate. *Chem. Commun.* **2012**, *48*, 4630−4632.
(38) Noguez, C.; Garzon, I. L. Optically active metal nanoparticles. *Chem. Soc. Rev.* **2009**, *38*, 757−71.
(39) Santizo, I. E.; Hidalgo, F.; Pérez, L. A.; Noguez, C.; Garzón, I. L. Intrinsic Chirality in Bare Gold Nanoclusters: The Au_{34}^- Case. *J. Phys. Chem. C* **2008**, *112*, 17533−17539.
(40) Lechtken, A.; Schooss, D.; Stairs, J. R.; Blom, M. N.; Furche, F.; Morgner, N.; Kostko, O.; von Issendorff, B.; Kappes, M. M. Au_{34}^-: a chiral gold cluster? *Angew. Chem., Int. Ed.* **2007**, *46*, 2944−2948.
(41) Garzón, I. L.; Reyes-Nava, J. A.; Rodríguez-Hernández, J. I.; Sigal, I.; Beltrán, M. R.; Michaelian, K. Chirality in bare and passivated gold nanoclusters. *Phys. Rev. B* **2002**, *66*, 073403.
(42) Häkkinen, H.; Moseler, M.; Kostko, O.; Morgner, N.; Hoffmann, M. v. Issendorff, B.: Symmetry and Electronic Structure of Noble-Metal Nanoparticles and the Role of Relativity. *Phys. Rev. Lett.* **2004**, 93.
(43) Wang, Z. W.; Palmer, R. E. Experimental evidence for fluctuating, chiral-type Au_{55} clusters by direct atomic imaging. *Nano Lett.* **2012**, *12*, 5510−5514.
(44) Sanchez-Castillo, A.; Noguez, C.; Garzon, I. L. On the origin of the optical activity displayed by chiral-ligand-protected metallic nanoclusters. *J. Am. Chem. Soc.* **2010**, *132*, 1504−1505.
(45) Tlahuice-Flores, A.; Whetten, R. L.; Jose-Yacaman, M. Ligand Effects on the Structure and the Electronic Optical Properties of Anionic $Au_{25}(SR)_{18}$ Clusters. *J. Phys. Chem. C* **2013**, *117*, 20867−20875.
(46) Lopez-Acevedo, O.; Tsunoyama, H.; Tsukuda, T.; Häkkinen, H.; Aikens, C. M. Chirality and electronic structure of the thiolate-protected Au_{38} nanocluster. *J. Am. Chem. Soc.* **2010**, *132*, 8210−8218.
(47) Malola, S.; Lehtovaara, L.; Knoppe, S.; Hu, K. J.; Palmer, R. E.; Bürgi, T.; Häkkinen, H. $Au_{40}(SR)_{24}$ cluster as a chiral dimer of 8-electron superatoms: structure and optical properties. *J. Am. Chem. Soc.* **2012**, *134*, 19560−19563.
(48) Pei, Y.; Gao, Y.; Zeng, X. C. Structural prediction of thiolate-protected Au_{38}: a face-fused bi-icosahedral Au core. *J. Am. Chem. Soc.* **2008**, *130*, 7830−7832.
(49) Knoppe, S.; Malola, S.; Lehtovaara, L.; Bürgi, T.; Häkkinen, H. Electronic Structure and Optical Properties of the Thiolate-Protected $Au_{28}(SMe)_{20}$ Cluster. *J. Phys. Chem. A* **2013**, *117*, 10526−10533.

(50) Nishida, N.; Yao, H.; Ueda, T.; Sasaki, A.; Kimura, K. Synthesis and Chiroptical Study of D/L-Penicillamine-Capped Silver Nanoclusters. *Chem. Mater.* **2007**, *19*, 2831−2841.
(51) Wu, Z.; Gayathri, C.; Gil, R. R.; Jin, R. Probing the structure and charge state of glutathione-capped $Au_{25}(SG)_{18}$ clusters by NMR and mass spectrometry. *J. Am. Chem. Soc.* **2009**, *131*, 6535−6542.
(52) Knoppe, S.; Dolamic, I.; Bürgi, T. Racemization of a Chiral Nanoparticle Evidences the Flexibility of the Gold-Thiolate Interface. *J. Am. Chem. Soc.* **2012**, *134*, 13114−13120.
(53) Varnholt, B.; Dolamic, I.; Knoppe, S.; Bürgi, T. On the flexibility of the gold-thiolate interface: racemization of the $Au_{40}(SR)_{24}$ cluster. *Nanoscale* **2013**, *5*, 9568−9571.
(54) Gautier, C.; Bürgi, T. Chiral gold nanoparticles. *ChemPhysChem* **2009**, *10*, 483−492.
(55) Xu, Q.; Kumar, S.; Jin, S.; Qian, H.; Zhu, M.; Jin, R. Chiral 38-Gold-Atom Nanoclusters: Synthesis and Chiroptical Properties. *Small* **2013**, DOI: 10.1002/smll.201302279.
(56) Tlahuice, A.; Garzon, I. L. Structural, electronic, optical, and chiroptical properties of small thiolated gold clusters: the case of Au_6 and Au_8 cores protected with dimer $[Au_2(SR)_3]$ and trimer $[Au_3(SR)_4]$ motifs. *Phys. Chem. Chem. Phys.* **2012**, *14*, 7321−7329.
(57) Nuzzo, R. G.; Zegarski, B. R.; Dubois, L. H. Fundamental studies of the chemisorption of organosulfur compounds on gold(111). Implications for molecular self-assembly on gold surfaces. *J. Am. Chem. Soc.* **1987**, *109*, 733−740.
(58) Love, J. C.; Estroff, L. A.; Kriebel, J. K.; Nuzzo, R. G.; Whitesides, G. M. Self-assembled monolayers of thiolates on metals as a form of nanotechnology. *Chem. Rev.* **2005**, *105*, 1103−1169.
(59) Grönbeck, H.; Curioni, A.; Andreoni, W. Thiols and Disulfides on the Au(111) Surface: The Headgroup−Gold Interaction. *J. Am. Chem. Soc.* **2000**, *122*, 3839−3842.
(60) Andreoni, W.; Curioni, A.; Grönbeck, H. Density functional theory approach to thiols and disulfides on gold: Au(111) surface and clusters. *Int. J. Quantum Chem.* **2000**, *80*, 598−608.
(61) Krüger, D.; Fuchs, H.; Rousseau, R.; Marx, D.; Parrinello, M. Interaction of short-chain alkane thiols and thiolates with small gold clusters: Adsorption structures and energetics. *J. Chem. Phys.* **2001**, *115*, 4776.
(62) Lavrich, D. J.; Wetterer, S. M.; Bernasek, S. L.; Scoles, G. Physisorption and Chemisorption of Alkanethiols and Alkyl Sulfides on Au(111). *J. Phys. Chem. B* **1998**, *102*, 3456−3465.
(63) Knoppe, S.; Michalet, S.; Bürgi, T. Stabilization of Thiolate-Protected Gold Clusters Against Thermal Inversion: Diastereomeric $Au_{38}(SCH_2CH_2Ph)_{24-2x}$(R-BINAS)$_x$. *J. Phys. Chem. C* **2013**, *117*, 15354−15361.
(64) Dass, A.; Stevenson, A.; Dubay, G. R.; Tracy, J. B.; Murray, R. W. Nanoparticle MALDI-TOF mass spectrometry without fragmentation: $Au_{25}(SCH_2CH_2Ph)_{18}$ and mixed monolayer $Au_{25}(SCH_2CH_2Ph)_{18-x}(L)_x$. *J. Am. Chem. Soc.* **2008**, *130*, 5940−5946.
(65) Niihori, Y.; Matsuzaki, M.; Pradeep, T.; Negishi, Y. Separation of Precise Compositions of Noble Metal Clusters Protected with Mixed Ligands. *J. Am. Chem. Soc.* **2013**, 4946−4949.
(66) Fields-Zinna, C. A.; Parker, J. F.; Murray, R. W. Mass Spectrometry of Ligand Exchange Chelation of the Nanoparticle $[Au_{25}(SCH_2CH_2C_6H_5)_{18}]^{1-}$ by $CH_3C_6H_3(SH)_2$. *J. Am. Chem. Soc.* **2010**, *132*, 17193−17198.
(67) Jupally, V. R.; Kota, R.; Van Dornshuld, E.; Mattern, D. L.; Tschumper, G. S.; Jiang, D. E.; Dass, A. Interstaple dithiol cross-linking in $Au_{25}(SR)_{18}$ nanomolecules: a combined mass spectrometric and computational study. *J. Am. Chem. Soc.* **2011**, *133*, 20258−20266.
(68) Knoppe, S.; Dass, A.; Bürgi, T. Strong non-linear effects in the chiroptical properties of the ligand-exchanged Au_{38} and Au_{40} clusters. *Nanoscale* **2012**, *4*, 4211−4216.
(69) Dass, A.; Holt, K.; Parker, J. F.; Feldberg, S. W.; Murray, R. W. Mass Spectrometrically Detected Statistical Aspects of Ligand Populations in Mixed Monolayer $Au_{25}L_{18}$ Nanoparticles. *J. Phys. Chem. C* **2008**, *112*, 20276−20283.
(70) Meng, X.; Xu, Q.; Wang, S.; Zhu, M. Ligand-exchange synthesis of selenophenolate-capped Au_{25} nanoclusters. *Nanoscale* **2012**, *4*, 4161−4165.
(71) Niihori, Y.; Kurashige, W.; Matsuzaki, M.; Negishi, Y. Remarkable enhancement in ligand-exchange reactivity of thiolate-protected Au_{25} nanoclusters by single Pd atom doping. *Nanoscale* **2013**, *5*, 508−512.
(72) Tang, Z.; Robinson, D. A.; Bokossa, N.; Xu, B.; Wang, S.; Wang, G. Mixed dithiolate durene-DT and monothiolate phenylethanethiolate protected Au_{130} nanoparticles with discrete core and core-ligand energy states. *J. Am. Chem. Soc.* **2011**, *133*, 16037−16044.
(73) Tang, Z.; Xu, B.; Wu, B.; Robinson, D. A.; Bokossa, N.; Wang, G. Monolayer reactions of protected au nanoclusters with monothiol tiopronin and 2,3-dithiol dimercaptopropanesulfonate. *Langmuir* **2011**, *27*, 2989−2996.
(74) Tang, Z.; Ahuja, T.; Wang, S.; Wang, G. Near infrared luminescence of gold nanoclusters affected by the bonding of 1,4-dithiolate durene and monothiolate phenylethanethiolate. *Nanoscale* **2012**, *4*, 4119−4124.
(75) Gautier, C.; Bürgi, T. Chiral Inversion of Gold Nanoparticles. *J. Am. Chem. Soc.* **2008**, *130*, 7078−7084.
(76) Knoppe, S.; Azoulay, R.; Dass, A.; Bürgi, T. In Situ Reaction Monitoring Reveals a Diastereoselective Ligand Exchange Reaction between the Intrinsically Chiral $Au_{38}(SR)_{24}$ and Chiral Thiols. *J. Am. Chem. Soc.* **2012**, *134*, 20302−20305.
(77) Knoppe, S.; Bürgi, T. The fate of $Au_{25}(SR)_{18}$ clusters upon ligand exchange with binaphthyl-dithiol: interstaple binding vs. decomposition. *Phys. Chem. Chem. Phys.* **2013**, *15*, 15816−15820.
(78) Molina, B.; Sanchez-Castillo, A.; Knoppe, S.; Garzon, I. L.; Bürgi, T.; Tlahuice-Flores, A. Structures and chiroptical properties of the BINAS-monosubstituted $Au_{38}(SCH_3)_{24}$ cluster. *Nanoscale* **2013**, *5*, 10956−10962.
(79) Beqa, L.; Deschamps, D.; Perrio, S.; Gaumont, A.-C.; Knoppe, S.; Bürgi, T. Ligand Exchange Reaction on $Au_{38}(SR)_{24}$, Separation of $Au_{38}(SR)_{23}(SR')_1$ Regioisomers, and Migration of Thiolates. *J. Phys. Chem. C* **2013**, *117*, 21619−21625.